Optics and Lasers in Engineering 66 (2015) 158–164

Contents lists available at ScienceDirect

Optics and Lasers in Engineering

journal homepage: www.elsevier.com/locate/optlaseng

Improved intensity-optimized dithering technique for 3D shape measurement

Jiasong Sun, Chao Zuo, Shijie Feng, Shiling Yu, Yuzhen Zhang, Qian Chen *

Jiangsu Key Laboratory of Spectral Imaging & Intelligence Sense, Nanjing University of Science and Technology, Nanjing, Jiangsu Province 210094, China

ARTICLE INFO

Article history:
Received 7 May 2014
Received in revised form
6 August 2014
Accepted 11 September 2014

Keywords:
3D shape measurement
Fringe analysis
Binary defocusing
Dithering
Optimization

ABSTRACT

The recently proposed optimized dithering techniques are able to improve measurement quality obviously. However, those phase-based optimization methods are sensitive to the amount of defocusing while intensity-based optimization methods cannot reduce the phase error efficiently. This paper presents a novel method, minimizing a proposed objective function named intensity residual error (IRE), as well as a novel framework, optimizing pixels group by group, to construct binary patterns for high-quality 3D shape measurement. Both the simulation and experimental results show that this proposed algorithm can achieve phase quality improvements over other recently optimized dithering techniques with various amounts of defocusing.

1. Introduction

With the recent advancement in digital display devices, three-dimensional (3D) scene acquisition becomes increasingly crucial in practical application fields of modern information technologies [1]. Among all the 3D non-contact shape measurement methods, digital fringe projection (DFP) methods have been considered as one of the most reliable techniques for recovering the shape of objects because of their accuracy and efficiency [2,3]. Since it is much easier and more convenient to generate and project the fringe patterns at a high speed with a commercial video projector, 3D shape measurement of dynamic objects such as high-speed moving objects and rotating bodies has been rapidly expanding [4–6]. However, the conventional DFP technique has the major limitations of the projection nonlinearity and speed bottleneck (i.e., typically 120 Hz) [7–9], making it difficult to apply to areas where capturing high-quality and high-speed deformation is required.

According to the operating principle of Digital Micro-mirror Device (DMD), projecting a binary pattern can break the projection speed bottleneck, increasing speed to a much higher frame rate (KHz). In addition, since binary pattern only has 1 bit depth, the nonlinearity problem of the projector can be solved easily. However, it is obvious that projecting binary pattern will bring about phase error comparing with projecting ideal sinusoidal fringe pattern. To reduce this phase error, some researchers employed a class of techniques that generates sinusoidal fringe patterns by rationally defocusing a coded binary pattern. Su et al. [10] introduced a technique for defocusing a square wave generated by the Ronchi grating for 3D shape measurement. After that, several techniques called squared binary defocusing method (SBM), sinusoidal pulse width modulation (SPWM), optimal pulse width modulation (OPWM) were proposed and developed which are generating sinusoidal fringe patterns by properly defocusing coded binary patterns using a digital video projector [8,11–14]. Compared to SBM, the SPWM and OPWM methods can produce better 3D shape measurement results especially when the defocusing degree is small. But the phase error caused by some unwanted high-order harmonics of the generated patterns of SPWM and OPWM methods is still non-negligible, especially when the projector is nearly focused [15].

Taking advantages of the two-dimensional (2D) nature of the structured patterns, area-modulation method could further improve the binary defocusing method [16]. And then, several 2D area dithering optimization methods are developed for phase-based DFP systems. These optimization methods can be classified into two categories: the intensity based method [17,18] and the phase-based method [19]. The former is to approximate the dithered pattern to ideal sinusoids after defocusing (e.g., applying a Gaussian filter) [17,18]. The latter is to make the phase close to the desired linear phase after defocusing [19]. Since the ultimate goal of optimization is to generate high-quality phase, it is natural to optimize the pattern in the phase domain. However, the phase-based optimization method is

* Corresponding author.
E-mail addresses: sjs0808402013@163.com (J. Sun), surpasszuo@163.com (C. Zuo), chenq_njust@163.com (Q. Chen).

http://dx.doi.org/10.1016/j.optlaseng.2014.09.008
0143-8166/

sensitive to different amounts of defocusing while the intensity-based optimization method cannot reduce the phase error efficiently.

Looking back at those one-dimensional (1D) pulse width modulation (PWM) methods [8,12–14], they either shift the high-order harmonics further away from fundamental frequency such that they are easier to be suppressed by defocusing [8], or theoretically eliminate those most influential harmonics [12–14]. The latter have proved that the three-step phase-shifting algorithm is insensitive to the presence of the $(3l)$th harmonics, where l is an integer [12]. Therefore, it is natural to optimize 2D area dithering methods in the intensity domain by taking advantage of this nice property.

This paper presents a new optimization method coming from our two observations: (1) for the phase-based optimization method, the intensity differences actually increase after optimization [18] and (2) the existence of the $(3l)$th harmonics does not induce any phase errors for the three-step phase-shifting algorithm [14]. Therefore, we defined an objective function named IRE which has removed the $(3l)$th harmonics out of the total intensity error between two patterns. The optimization is to minimize the IRE between the defocused (or blurred) binary pattern and the ideal sinusoidal pattern. Besides, instead of optimizing the whole pattern pixel by pixel, our framework is optimizing the pixels group by group to find the best smallest binary patches, and then tiling the best patch to generate the full-size pattern utilizing periodicity structure of the sinusoidal pattern. Both simulations and experiments demonstrate that the proposed method can achieve substantial phase quality improvements when the projector is at different amounts of defocusing especially when the fringe period is larger.

This paper is organized as follows: Section 2 explains the principle of the three-step phase-shifting algorithm and the proposed definition of IRE. Section 3 presents the proposed framework for constructing binary patterns. Section 4 shows simulation results. Section 5 presents the experimental results. Section 6 discusses the merits and shortcomings of the proposed technique, and finally Section 7 summarizes this paper.

2. Principle

2.1. Three-step phase-shifting algorithm

Phase-shifting algorithms have been extensively used in optical metrology. Typically, the more fringe patterns used, the better measurement quality can be achieved. For high-speed 3D shape measurement, a three-step phase-shifting algorithm is usually adopted since it requires the minimum number of patterns to solve the phase. As our research focuses on high-speed 3D shape measurement, a simple three-step phase-shifting algorithm with a phase shift of $2\pi/3$ is used to test the generated patterns. Three ideal fringe images can be described as

$$I_1(x,y)=I'(x,y)+I''(x,y)\ \cos\left(\phi(x,y)-\frac{2\pi}{3}\right), \tag{1}$$

$$I_2(x,y)=I'(x,y)+I''(x,y)\ \cos(\phi(x,y)), \tag{2}$$

$$I_3(x,y)=I'(x,y)+I''(x,y)\ \cos\left(\phi(x,y)+\frac{2\pi}{3}\right), \tag{3}$$

where $I'(x,y)$ is the average intensity, $I''(x,y)$ the intensity modulation, and $\phi(x,y)$ the phase to be solved for

$$\phi(x,y)=\tan^{-1}\frac{\sqrt{3}(I_1(x,y)-I_3(x,y))}{2I_2(x,y)-I_1(x,y)-I_3(x,y)}. \tag{4}$$

This equation provides the wrapped phase ranging $[-\pi,\pi)$ with 2π discontinuities [20,21]. A continuous phase map can be obtained by adopting a temporal [20] or spatial phase unwrapping algorithm [21]. Considering a typical temporal phase unwrapping algorithm, a continuous phase map is obtained by using six patterns, two frequencies [20]. Recently, several temporal phase unwrapping strategies have been developed, and the number of required patterns has been reduced to four or five, shortening the pattern sequence required for unwrapping phase images [9,13]. In this research, we use the traditional temporal phase unwrapping framework with six patterns [20].

2.2. Optimization based on the IRE

As explained previously, obtaining high-quality phase is extremely important for high-quality 3D shape measurement. Meanwhile, two phenomena got our attention: (1) for the phase-based optimization method, the intensity differences actually increase after optimization [18] and (2) the existence of the $(3l)$th harmonics does not induce any phase errors for the three-step phase-shifting algorithm [14]. Therefore, it can be proved that if the intensity error varies periodically at the frequency which is multiple of $3f_0$ (f_0 is the fundamental frequency of the desired sinusoidal pattern), the obtained phase map could be as same as the ideal phase map. Assume that the desired sinusoidal fringe patterns vary along the x direction for one fringe period (T). For the three-step phase-shifting algorithm, when the fringe period is multiple of 3, like $T=3N(N=3,4,5\ldots)$, there is a relation between three fringe patterns: $I_1(x-N,y)=I_2(x,y)=I_3(x+N,y)$. That means only one fringe pattern has to be generated, and the other two patterns can be realized by shifting the first pattern. Therefore, fringe period (T) is usually chosen to be a multiple of 3 to avoid phase-shift error for the three-step phase-shifting algorithm [12], and three defocused fringe images can be described as

$$D_1(x,y)=I_1(x,y)+E_1(x,y), \tag{5}$$

$$D_2(x,y)=I_2(x,y)+E_2(x,y), \tag{6}$$

$$D_3(x,y)=I_3(x,y)+E_3(x,y), \tag{7}$$

where $D_i(x,y)$ are the defocused fringe patterns, $I_i(x,y)$ are the ideal sinusoidal intensity patterns, $E_i(x,y)$ represent the intensity error maps between them ($i=1,2,3$). Assume that the intensity error varies periodically along the x direction for one column period $S_x(S_x=T/3=N)$, and then we can get

$$E_1(x,y)=E_2(x-N,y)=E_2(x,y)=E_2(x+N,y)=E_3(x,y). \tag{8}$$

Therefore, $\phi'(x,y)$ the obtained phase map to be solved for

$$\begin{aligned}\phi'(x,y)&=\tan^{-1}\frac{\sqrt{3}(D_1(x,y)-D_3(x,y))}{2D_2(x,y)-D_1(x,y)-D_3(x,y)}\\&=\tan^{-1}\frac{\sqrt{3}(I_1(x,y)-I_3(x,y))}{2I_2(x,y)-I_1(x,y)-I_3(x,y)}=\phi(x,y).\end{aligned} \tag{9}$$

It is obvious that the obtained phase map just equate to the ideal phase map. Unfortunately, the intensity error could not vary periodically at the frequency which is multiple of $3f_0$ actually. But it is possible to separate the $(3l)$th harmonics out of the total intensity error. Therefore, mathematically we defined an IRE $E_r(x,y)$ described as

$$E_r(x,y)=E(x,y)-E_{3f_0}(x,y), \tag{10}$$

$$E(x,y)=G(x,y)*B(x,y)-I(x,y), \tag{11}$$

where $E(x,y)$ is the total intensity error between the defocused binary pattern and the ideal sinusoidal pattern, $E_{3f_0}(x,y)$ is the periodically $(3l)$th harmonics, $G(x,y)$ is a 2D Gaussian kernel, $B(x,y)$ is the desired 2D binary pattern, and $*$ represents convolution, $I(x,y)$ is the ideal sinusoidal intensity pattern. The optimization we proposed is to minimize the IRE $E_r(x,y)$. This is the most

fundamental difference between our algorithm and other previously developed algorithms [17]. Mathematically, the optimization problem can be described as the following function:

$$\min_B \|E_r(x,y)\|_F = \min_B \|G(x,y)*B(x,y) - I(x,y) - E_{3f_0}(x,y)\|_F, \tag{12}$$

where $\|\cdots\|_F$ represents the Frobenius norm. Typically, it is natural to employ Discrete Fourier Transform (DFT) to extract the $(3l)$th harmonics $E_{3f_0}(x,y)$ out of the total intensity error $E(x,y)$. But in that way, two times of spatial-frequency transform should be made, and it is complicated to some extent. So we present a simple way to accomplish this extraction without spatial-frequency transform in the following section.

2.3. Extraction of the $(3l)$th harmonics

Assume that a periodical signal $s(x)$ vary along the x direction for one period $T(T=3N)$, and $s_{3N}(x)(x=0,1,2,3,\ldots,3N-1)$ is one period segment of $s(x)$. In order to extract the $(3l)$th harmonics $s_N(x)$ of the whole signal $s_{3N}(x)$, it is natural to employ DFT on $s_{3N}(x)$ to obtain its spectrum $S_{3N}(k)(k=0,1,2,3,\ldots,3N-1)$. After that, all those harmonics at the frequency $3l(l=0,1,2,3,\ldots,N-1)$ should be retained, and other harmonics should be removed. Therefore, the new sampled spectrum $S_N(k)$ can be described as

$$S_N(k) = S_{3N}(k)\cdot H(k), \tag{13}$$

$$H(k) = \frac{1}{3}comb\left(\frac{k}{3}\right) = \frac{1}{3}\sum_{l=0}^{N-1}\delta\left(\frac{k}{3}-l\right) = \sum_{l=0}^{N-1}\delta(k-3l), \tag{14}$$

where $H(k)$ is the sampling function, also named as Dirac comb function, every δ function separating from each other at 3. According to the DFT theory and convolution principle, mathematically this filtering process in the spatial domain can be described as

$$s_N(x) = s_{3N}(x)*h(x), \tag{15}$$

$$h(x) = \frac{1}{3N}comb\left(\frac{x}{N}\right) = \frac{1}{3N}\sum_{m=0}^{2}\delta\left(\frac{x}{N}-m\right) = \frac{1}{3}\sum_{m=0}^{2}\delta(x-Nm), \tag{16}$$

where $h(x)$ is the spatial filtering function corresponding to $H(k)$, $*$ represents convolution. It turns out that $h(x)$ is a Dirac comb function either, but it is composed of three δ functions and the extent decreases to $1/3$. Therefore, $s_N(x)$ the $(3l)$th harmonics to be solved for

$$s_N(x) = s_{3N}(x)*\frac{\delta(x)+\delta(x-N)+\delta(x-2N)}{3} = \frac{s_{3N}(x)+s_{3N}(x-N)+s_{3N}(x-2N)}{3}. \tag{17}$$

Therefore, utilizing this method, the extraction of the $(3l)$th harmonics $E_{3f_0}(x,y)$ out of the total intensity error $E(x,y)$ can be described as the following function:

$$E_{3f_0}(x,y) = \frac{1}{3}\left[E(x,y)+E\left(x+\frac{T}{3},y\right)+E\left(x+\frac{2T}{3},y\right)\right]. \tag{18}$$

This function demonstrates a simple way to extract the $(3l)$th harmonics $s_N(x)$ out of signal $s_{3N}(x)$ without DFT. Firstly, $s_{3N}(x)$ is divided into three segments at the same length N. Secondly, add three segments together to calculate an average segment. And finally, the $(3l)$th harmonics $s_N(x)$ is generated by periodically extending the average segment along the x direction three times.

Then, IRE $E_r(x,y)$ can be obtained by utilizing Eqs. (10), (11) and (18).

3. Binary pattern construction framework

Instead of solving the whole NP-hard problem equation (12) (e.g., 800×600), we use a method to solve subset problem: namely obtain a subset called the best patch, and then tile the best patch to generate the full-size patterns utilizing periodicity.

As described in Eq. (4), the phase of one pixel is determined by the intensity of three pixels at an interval of $T/3$ along the x direction. Therefore, all pixels of the patch can be classified into several groups according to the following order. There are three pixels in a group and two of them are apart from the center pixel at $T/3$ (or $-T/3$) along the x direction. After classification, pixels are mutated group by group, instead of mutating one by one. This is another fundamental difference between our algorithm and other previously developed algorithms [17]. The main steps of the proposed algorithm are as follows:

Step 1: Patch initialization: This step initializes the patch size by the row period $S_y(S_y=1)$ and the column period S_x, and assign each pixel of the patch with random binary value 0 (or 1). Here $S_x=T$ is one fringe period.

Step 2: Pixel mutation: All pixels are classified into several groups according to the classification order. After classification, three pixels in the first group are mutated to their opposite status (1 s are changed to 0 s and 0 s are changed to 1 s). According to the enumerative algorithm (such as $(0,0,0),(0,0,1),(0,1,0),(0,1,1),(1,0,0),(1,0,1),(1,1,0),(1,1,1)$), all eight patches are generated. Among these eight patches, only the "*good*" patch is kept. The "*good*" patch means that the matrix B can minimize Eq. (12). Then, mutate other pixels group by group until every group has been mutated. In this step, the algorithm uses a small Gaussian filter (size: 5×5 pixels and standard deviation 2 pixels) to emulate the slightly defocused projector.

Step 3: Iteration: This whole algorithm needs to be performed iteratively since if one of the pixels is altered, its neighboring pixels would also be affected after Gaussian smoothing. Therefore, after obtaining the whole patch, it would go back to the previous Step 2 until the algorithm converges. The convergence rule we proposed to use is that the improvement of intensity residual root mean square (RMS) error for a round of processing is less than 0.01%.

Step 4: Patch size mutation: Change S_y to another value (2–16), and go to Steps 2–3 to generate another "*good*" patch for different patch size. Here we suggest that the row period S_y does not vary above 16 because when S_y become larger, the phase quality does not improve efficiently while multiplying the time consuming in optimizing.

Step 5: Patch selection: Select the "*better*" patch from the set of "*good*" patches generated from Steps 2 to 4. The "*better*" patch means that the matrix B can minimize Eq. (12) among all these sixteen "*good*" patches.

Step 6: Gaussian filter size mutation: In order to simulate different amount of defocusing, we propose to change the small Gaussian filter into a medium Gaussian filter (size: 9×9 pixels and standard deviation 3 pixels) or a large Gaussian filter (size: 13×13 pixels and standard deviation 4 pixels). They were used to emulate the defocused projector with two different amount of defocusing. And then go back to Steps 1–5 to generate other two "*better*" patches.

Step 7: Final patch selection. After Step 6, three "*better*" patches have been generated. From these patches, the final *best* patch was selected based on the following two rules: (1) the average phase RMS error is lower than others' when different sizes of Gaussian filters are applied and (2) the phase error is not sensitive to different sizes of Gaussian filters. In addition, the first rule has priority.

Step 8: Full-size pattern generation: Utilizing the periodicity properties of ideal fringe pattern, the desired size fringe pattern was generated by periodically extending the final *best* patch along x and y directions.

In order to explain how to select the final best patch to be used in Step 7, some examples are given. Fig. 1(a)–(c) shows a set of three better patches generated after Steps 1–6 when fringe period $T=36$. Fig. 1(d) shows the phase RMS error of these three patches with different amounts of defocusing. Pattern 1 performs the best when the amount of defocusing is smaller (Gaussian filter size 5×5), but does not perform well with larger amount of defocusing. Pattern 2 depicts the smallest phase RMS error when the filter size is 9×9, and it performs consistently over different amounts of defocusing. Since the average phase RMS errors of these two patterns are quite close and Pattern 2 performs consistently, Pattern 2 is regarded as a better candidate. Pattern 3 depicts the smallest phase RMS error when the filter size is 13×13, and it performs extremely sensitive to different amounts of defocusing. However, considering all these phase RMS errors of three patterns, Pattern 3 performs best on average. Therefore, according to the pattern selection rules mentioned in Step 7, Pattern 3 is chosen as the final best patch to be used.

It seems strange that Pattern 3 is the square binary pattern but it still can obtain an acceptable phase quality after defocusing, even better than other optimized patterns. This is because of that when the fringe period of a pattern is small, an appropriate Gaussian filter can filter out all those high-frequency harmonics (frequency above $3f_0$), and the residual third harmonics do not induce any phase errors for the three-step phase-shifting algorithm. Therefore, the square binary patterns are chosen as the final best patches when the fringe periods of them are small and the projector is more defocused.

4. Simulations

We simulated different amounts of defocusing by applying different sizes of Gaussian filters. The smallest Gaussian filter was 5×5 with a standard deviation of 2 pixels, and the largest was 13×13 with a standard deviation of 4 pixels. A Gaussian filter size of 5×5 represents the case that the projector is slightly defocused, while 13×13 represents the case when the projector is defocused to a much more degree.

Fig. 2 shows the simulation results. The simulation results clearly show that the proposed method can substantially improve

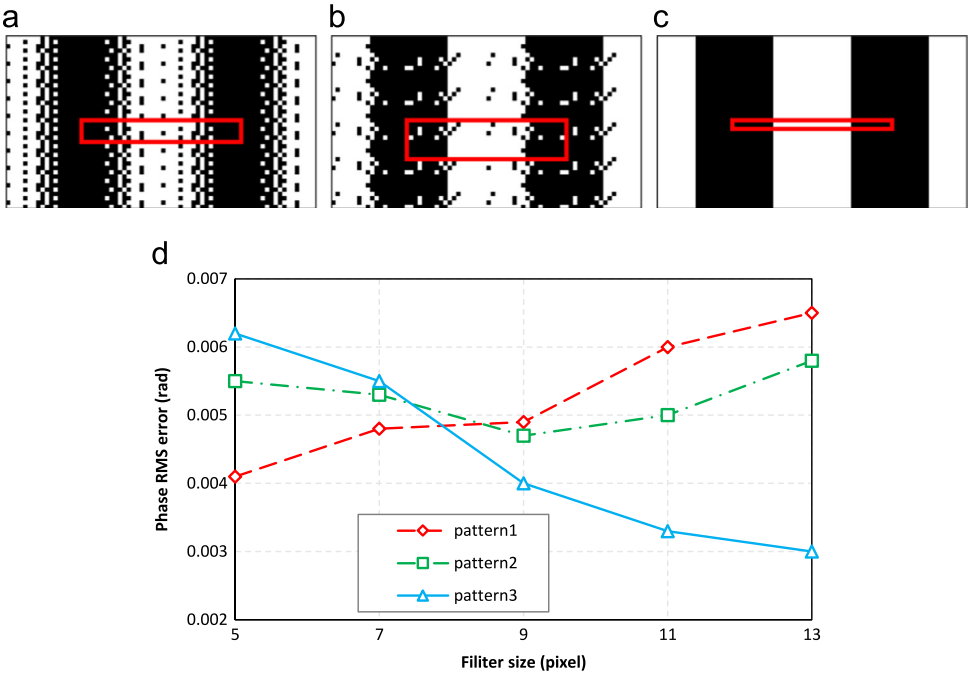

Fig. 1. Example of selecting the pattern from the optimized binary patches. (a) Pattern 1: $T=36$, Sy$=4$; (b) pattern 2: $T=36$, Sy$=8$; (c) pattern 3: $T=36$, Sy$=1$; (d) phase RMS error with different amounts of defocusing.

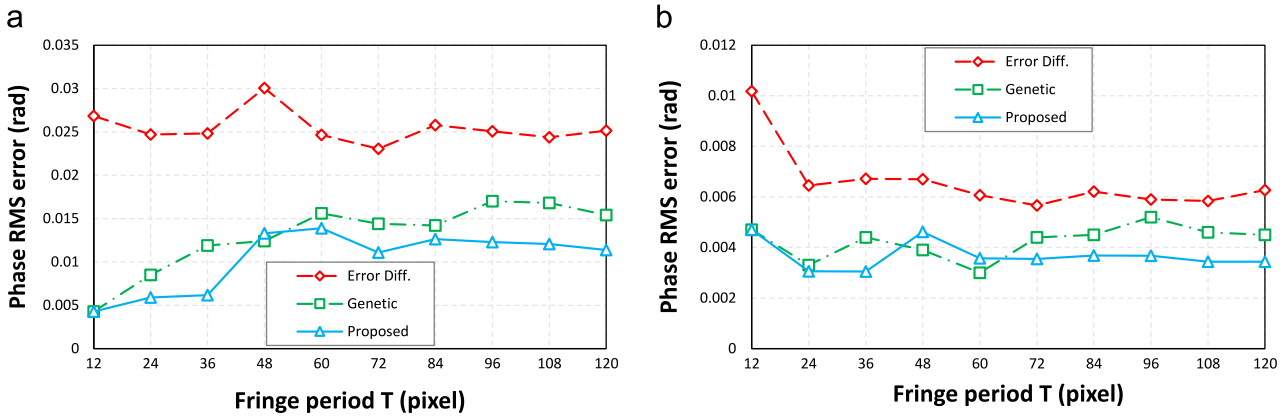

Fig. 2. Comparing the phase quality among the proposed method, the genetic method and the error-diffusion technique. (a) Gaussian filter size of 5×5 pixels and standard deviation of 2 pixels; (b) Gaussian filter size of 13×13 pixels and standard deviation of 4 pixels.

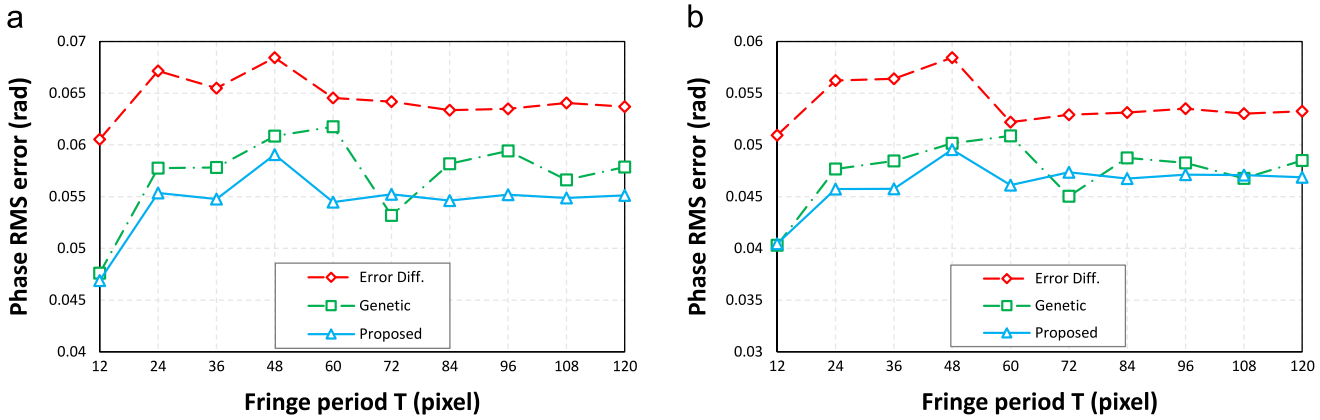

Fig. 3. Experimentally comparing the phase quality among the proposed method, the genetic method, and the error-diffusion technique. (a) Slightly defocused; (b) more defocused.

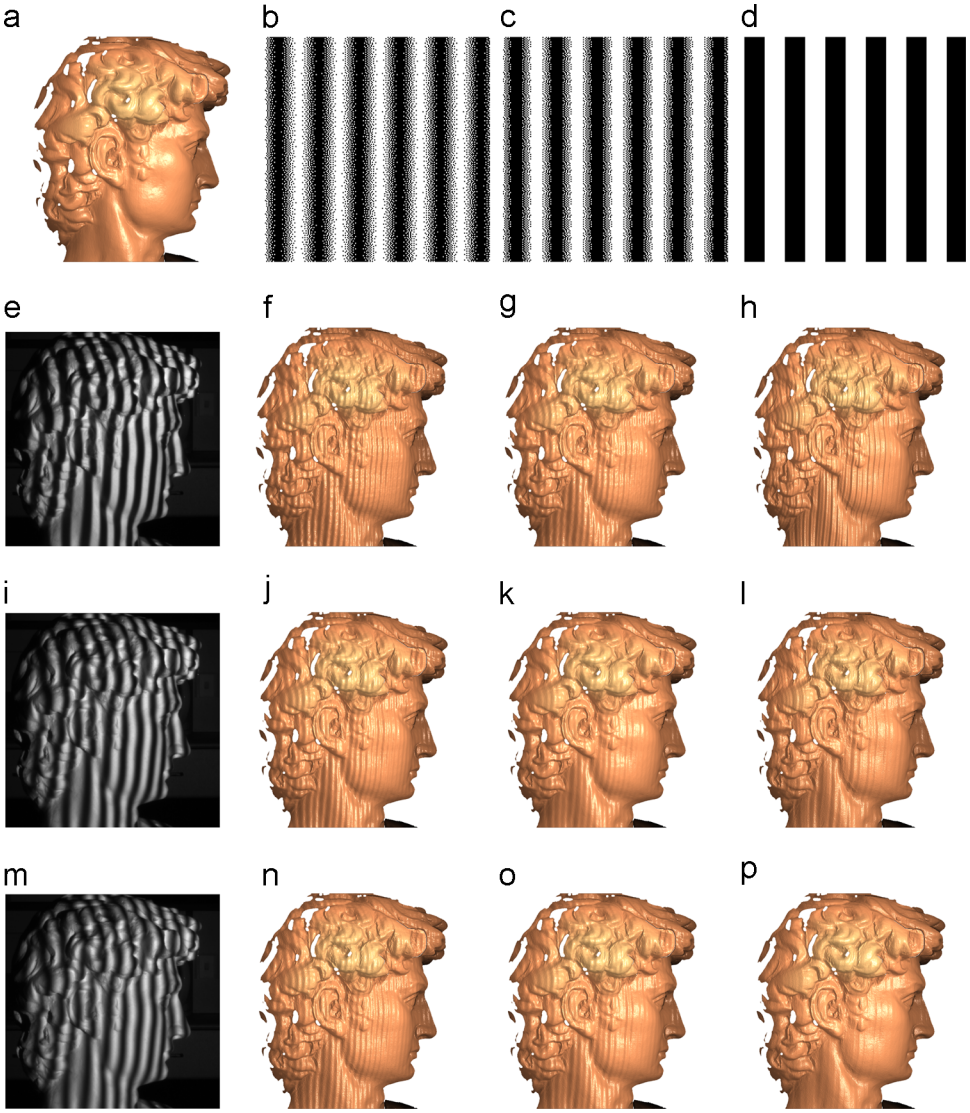

Fig. 4. Measurement results of a complex 3D statue. (a) The ideal 3D shape of the complex statue; (b), (c), and (d) show three binary patterns used in the experiment, which were respectively generated by utilizing the error-diffusion method, the genetic method, and the proposed method; (e), (i), and (m) show three defocused patterns generated by utilizing the proposed method in different amount of defocusing respectively, which are nearly focused, slightly defocused, and more defocused; (f)–(h), (j)–(l), and (n)–(p) show the 3D result when the projector is nearly focused, slightly defocused, and more defocused respectively. Each column represents one different dithering technique, which is the error-diffusion method, the genetic method or the proposed method.

the fringe quality for different amounts of defocusing. Compared with the genetic method, it also indicates that when the fringe period increases, the improvement of our method is larger and performs consistently. This demonstrates the success of our algorithm, and it is the fundamental improvement over other previously developed algorithms.

5. Experiments

We also conducted experiments to verify the performance of the proposed technique. The 3D shape measurement system includes a modified DLP commercial projector (ACER X1161PA) having the resolution of 800 × 600 pixels, a high speed industrial CCD camera GE680 (Allied Vision Technologies) with the resolution of 640 × 480 pixels.

We experimentally verified the simulation results by measuring a flat white board using all these fringe patterns. Fig. 3 shows the results. The phase errors were determined by taking the difference between the phase obtained from the defocused binary patterns (the error-diffusion patterns, the genetic patterns, and the proposed patterns) and the phase obtained from the ideal sinusoidal patterns. Again, the results generated by the proposed algorithm are better than the results generated by the error-diffusion algorithm, and the genetic algorithm at different amounts of defocusing especially when the fringe period is larger than 48 pixels.

A more complex 3D statue was measured to compare these methods. Fig. 4(b), (c), and (d) shows three binary patterns used in the experiment, which were respectively generated by utilizing the error-diffusion method, the genetic method, and the proposed method. In this experiment, we used the fringe period of $T=36$ pixels, and unsurprisingly the pattern generated by our proposed method is a square binary pattern as we have discussed in the last paragraph in Section 3. In order to compare these methods quantitatively, the same 3D statue was measured by the same system, with the 16-step phase-shifting method and ideal sinusoidal patterns. Then we assumed that this result shown in Fig. 4(a) was exactly the 3D shape of the complex statue. Finally, the phase RMS errors of these three dithering methods, corresponding to Fig. 4(f)–(h), (j)–(l), and (n)–(p), were calculated which in order are 0.0592 rad, 0.0567 rad, and 0.0597 rad for nearly focused patterns, 0.0574 rad, 0.0550 rad, and 0.0547 rad for slightly defocused patterns, 0.0537 rad, 0.0518 rad, and 0.0459 rad for more defocused patterns respectively. Clearly, these numbers demonstrate that at larger amounts of defocusing, the proposed method is much better than the error-diffusion method and the genetic method. Furthermore, visually, it is easy to tell the improvement of the proposed method in Fig. 4. Again, the experiment results show that the square binary patterns can achieve higher measurement quality than other patterns generated by some optimization methods when the fringe period is small, and the projector is at an appropriate extent of defocusing.

However, the square binary pattern cannot obtain an acceptable phase quality after defocusing for every fringe period. Fig. 5 shows the measurement results when fringe period $T=48$ pixels, and the projector was at the same extent of defocusing in Fig. 4(p). These results clearly show that when the fringe period is larger than 48, the proposed pattern performs better than the square binary pattern. Because there are much more high-frequency harmonics (frequency above $3f_0$) in the square binary pattern after defocusing. In addition, the phase RMS errors of these two results, corresponding to Fig. 5(c) and (f), were calculated which are 0.0515 rad and 0.0665 rad respectively.

6. Discussions

Compared with all those previous optimization method along the same direction [17,19], this proposed method is fundamentally different from any of them, where they either modified the dithered patterns to minimize the original intensity error or phase error, or mutated the error pixels one by one. The proposed technique, in contrast, optimizes patterns by minimizing the IRE, and mutating pixels group by group. Taking advantage of the insensitivity between the three-step phase-shifting algorithm and the $(3l)$th harmonics, the proposed algorithm can obtain high-quality phase map for different amounts of defocusing, over performing those optimization methods proposed previously. In addition, it is easier to be realized

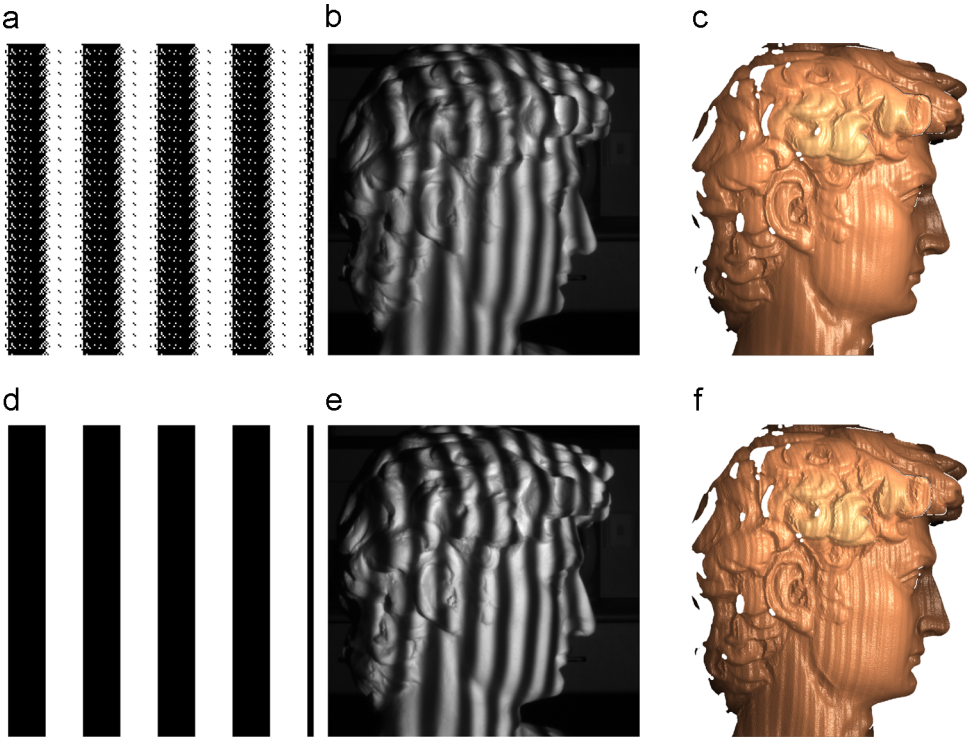

Fig. 5. Measurement results of a complex 3D statue when fringe period $T=48$ pixels. (a) and (d) respectively show the proposed pattern and the square binary pattern; (b) and (e) respectively show two defocused patterns corresponding to (a) and (d); (c) and (f) respectively show the 3D measurement result utilizing the proposed pattern and the square binary pattern when the projector is at large amounts of defocusing.

on hardware since the element used is very small, instead of storing the whole pattern (e.g., 800×600).

However, if the fringe period (T) is not multiple of 3, for example $T=16$ or $T=25$, the relation between three fringe patterns still exists: $I_1(x-T/3,y)=I_2(x,y)=I_3(x+T/3,y)$. But $T/3$ is no longer an integer, which means three different fringe patterns cannot be generated by shifting one of them. Unfortunately, in our proposed method, this shifting property of three fringe patterns is a precondition for the extraction of the third harmonics and the optimization framework. Therefore, our improved method cannot be utilized for three-step phase-shifting algorithm when fringe period (T) is not multiple of 3. In other words, generally this method only can be utilized for N-step phase-shifting algorithm when fringe period (T) is multiple of N. This seems to be a limitation of the proposed method.

Besides, the proposed algorithm consumes much time, even hours, when generating the final best patch for wider fringe stripe, whose fringe period is above 60 pixels. This seems to be another limitation of our proposed method.

7. Conclusion

This paper has presented an improved optimization method based on the IRE to generate high-quality sinusoidal fringe patterns with binary patterns. We found that this method could improve the phase quality efficiently for different amounts of defocusing especially for wider fringe stripes. Both simulation and experimental results demonstrated the success of the proposed technique.

Acknowledgments

This project was supported by the Research Fund for the Doctoral Program of Ministry of Education of China (No. 20123219110016), the Research and Innovation Plan for Graduate Students of Jiangsu Higher Education Institutions, China (No. CXLX13_177), the National Natural Science Foundation of China (No. 61271332) and the Open Research Fund of Jiangsu Key Laboratory of Spectral Imaging & Intelligent Sense.

References

[1] Chen F, Brown GM, Song M. Overview of three-dimensional shape measurement using optical methods. Opt Eng 2000;39:10–22.
[2] Gorthi SS, Rastogi P. Fringe projection techniques: whither we are?. Opt Lasers Eng 2010;48:133–40.
[3] Feng S, Zhang Y, Chen Q, Zuo C, Li R, Shen G. General solution for high dynamic range three-dimensional shape measurement using the fringe projection technique. Opt Lasers Eng 2014;59:56–71.
[4] Zhang Q, Su X. High-speed optical measurement for the drumhead vibration. Opt Express 2005;13:3110–6.
[5] Zhang Q, Su X, Cao Y, Li Y, Xiang L, Chen W. Optical 3-d shape and deformation measurement of rotating blades using stroboscopic structured illumination. Opt Eng 2005;44:113601.
[6] Feng S, Chen Q, Zuo C, Li R, Shen G, Feng F. Automatic identification and removal of outliers for high-speed fringe projection profilometry. Opt Eng 2013;52:013605.
[7] Zhang S, Yau S-T. High-resolution, real-time 3d absolute coordinate measurement based on a phase-shifting method. Opt Express 2006;14:2644–9.
[8] Ayubi GA, Ayubi JA, Di Martino JM, Ferrari JA. Pulse-width modulation in defocused three-dimensional fringe projection. Opt Lett 2010;35:3682–4.
[9] Zuo C, Chen Q, Gu G, Feng S, Feng F. High-speed three-dimensional profilometry for multiple objects with complex shapes. Opt Express 2012;20:19493–510.
[10] Su X, Zhou W, Von Bally G, Vukicevic D. Automated phase-measuring profilometry using defocused projection of a Ronchi grating. Opt Commun 1992;94:561–73.
[11] Wang Y, Zhang S. Optimal pulse width modulation for sinusoidal fringe generation with projector defocusing. Opt Lett 2010;35:4121–3.
[12] Zuo C, Chen Q, Feng S, Feng F, Gu G, Sui X. Optimized pulse width modulation pattern strategy for three-dimensional profilometry with projector defocusing. Appl Opt 2012;51:4477–90.
[13] Zuo C, Chen Q, Gu G, Feng S, Feng F, Li R, et al. High-speed three-dimensional shape measurement for dynamic scenes using bi-frequency tripolar pulse-width-modulation fringe projection. Opt Lasers Eng 2013;51:953–60.
[14] Zuo C, Chen Q, Gu G, Ren J, Sui X, Zhang Y. Optimized three-step phase-shifting profilometry using the third harmonic injection. Opt Appl 2013;51:393–408.
[15] Wang Y, Zhang S. Comparison of the squared binary, sinusoidal pulse width modulation, and optimal pulse width modulation methods for three-dimensional shape measurement with projector defocusing. Appl Opt 2012;51:861–72.
[16] Xian T, Su X. Area modulation grating for sinusoidal structure illumination on phase-measuring profilometry. Appl Opt 2001;40:1201–6.
[17] Lohry W, Zhang S. Genetic method to optimize binary dithering technique for high-quality fringe generation. Opt Lett 2013;38:540–2.
[18] Dai J, Li B, Zhang S. Intensity-optimized dithering technique for three-dimensional shape measurement with projector defocusing. Opt Lasers Eng 2014;53:79–85.
[19] Dai J, Zhang S. Phase-optimized dithering technique for high-quality 3d shape measurement. Opt Lasers Eng 2013;51:790–5.
[20] Li J, Hassebrook LG, Guan C. Optimized two-frequency phase-measuring-profilometry light-sensor temporal-noise sensitivity. JOSA A 2003;20:106–15.
[21] Ghiglia DC, Pritt MD. Two-dimensional phase unwrapping: theory, algorithms, and software. New York: Wiley; 1998.